Antibiotic-decorated titanium with enhanced antibacterial activity through adhesive polydopamine for dental/bone implant

Shu He[1,†], Ping Zhou[3,†], Linxin Wang[4], Xiaoling Xiong[1], Yifei Zhang[2], Yi Deng[3] and Shicheng Wei[1,3]

[1]Department of Oral and Maxillofacial Surgery, Laboratory of Interdisciplinary Studies, and [2]Central Laboratory, School and Hospital of Stomatology, Peking University, Beijing 100081, People's Republic of China
[3]Center for Biomedical Materials and Tissue Engineering, Academy for Advanced Interdisciplinary Studies, Peking University, Beijing 100871, People's Republic of China
[4]Department of Stomatology, Beijing Shijitan Hospital, Capital Medical University, Beijing 100038, People's Republic of China

Implant-associated infections, which are normally induced by microbial adhesion and subsequent biofilm formation, are a major cause of morbidity and mortality. Therefore, practical approaches to prevent implant-associated infections are in great demand. Inspired by adhesive proteins in mussels, here we have developed a novel antibiotic-decorated titanium (Ti) material with enhanced antibacterial activity. In this study, Ti substrate was coated by one-step pH-induced polymerization of dopamine followed by immobilization of the antibiotic cefotaxime sodium (CS) onto the polydopamine-coated Ti through catechol chemistry. Contact angle measurement and X-ray photoelectron spectroscopy confirmed the presence of CS grafted on the Ti surface. Our results demonstrated that the antibiotic-grafted Ti substrate showed good biocompatibility and well-behaved haemocompatibility. In addition, the antibiotic-grafted Ti could effectively prevent adhesion and proliferation of *Escherichia coli* (Gram-negative) and *Streptococcus mutans* (Gram-positive). Moreover, the inhibition of biofilm formation on the antibiotic-decorated Ti indicated that the grafted CS could maintain its long-term antibacterial activity. This modified Ti substrate with enhanced antibacterial activity holds great potential as implant material for applications in dental and bone graft substitutes.

1. Introduction

Hospital-acquired infections have been on the rise in the past decade with staggering numbers. It is reported that about 1.7 million hospitalized patients were afflicted by nosocomial infections in 2002, of which almost 100 000 cases resulted in fatalities [1]. Almost half of nosocomial infections are device-related, with the greatest percentage of cases consisting of implant infections. However, over recent years, there has been a marked increase in demand for implants, especially for dental and bone applications as a replacement for soft and hard tissue [2]. Titanium and titanium-based alloys with excellent properties (load-bearing, low density and biocompatibility) have been widely used as artificial implants in dental, bone replacement and orthopaedic surgery [3]. Nevertheless, there have been some cases of Ti implant failure [4–6], which are costly to rectify and are often distressing for the patients.

Microbial infection is one of the main causes of implant failure [4,5]. During the process of surgery, implants are susceptible to bacterial contamination on skin and mucous membranes [6]. These device-associated infections can progress rapidly as planktonic bacteria first adhere to an implant interface and ultimately evolve into biofilms [7]. Bacteria in the biofilm can reduce metabolic activities,

form extracellular polymer matrix to defend against harmful environmental physical and chemical factors, evade host immunological surveillance and hinder the diffusion and permeation of antibiotics [8,9]. Lack of antibacterial activity on the implant–abutment interface often causes undesirable complications such as oral infections and inflammatory reactions. Additionally, an infection caused by biofilm is not easy to remove, causing the destruction of the adjacent tissue, and implant loosening or even detachment [10]. Therefore, it is critical to reduce and eventually eliminate the infection on the dental/bone implants.

A great deal of research has been focused on preventing biofilm formation onto implant interfaces in recent years [11,12]. Surface functionalization is a relatively straightforward method for modifying the interfacial properties of medical devices without disrupting the bulk properties of material. It can also prevent device-associated infections *in vivo* at the implantation sites where antibiotics cannot reach [13]. Many antibacterial polymers [14,15], antimicrobial peptides [16,17], silver ion [18] and antibiotics [19,20] have been actively investigated to improve the antibacterial activity of implant materials. Diverse approaches, including physical adsorption and chemical covalent conjugation, have been applied to immobilize antimicrobial materials onto implant interfaces. Antibiotics, such as nitrofurazone [19] and minocycline/rifampicin [21], were reported to be impregnated onto implant devices. This method can partially reduce bacterial adhesion and biolm formation; however, the antimicrobial effectiveness is largely dependent on the continuous release of the impregnated agents, and their usage may be limited to the short term. Covalent bonding of biocompatible antibacterial agents onto the implant interface appears promising, because agents will not be released, and efficacy can be maintained for long-term application [22]. Typical chemical conjugation methods, on the other hand, require complicated and multi-step procedures such as surface activation or functionalization steps requiring plasma or chemical treatments [23]. Nevertheless, denaturation of bioactive agents by toxic chemicals and multiple reaction steps may restrict their applications in clinic [23,24]. Therefore, there is a pressing need to develop a non-toxic, facile and effective implant modification method for prevention of infections on the implant interface.

Cefotaxime sodium (CS), a broad spectrum antibiotic, is widely used in treatment of susceptible infections in respiratory tract, skin and skin structure without serious side effects, and it has good activity against Gram-positive and Gram-negative bacteria [25,26]. Dopamine, a mussel-inspired molecule, can undergo self-polymerization and adhere onto almost any solid surface without surface pre-treatments. More importantly, polydopamine (pDA) coating can function as an anchor to graft secondary functional biopolymers by thiols and amines via Michael addition or Schiff base reactions [27–29]. In this study, we present a novel CS-decorated Ti implant with antibacterial activity through adhesive dopamine for the first time. The effects of the CS-decorated Ti on bacteria proliferation and biofilm formation were investigated. Because of the known problems regarding the acquired resistance of bacteria, further comprehensive fabrication and evaluation of various antibiotic-decorated Ti implants are currently underway in our laboratory. The presented facile, green and effective method endows the Ti implant with enhanced antibacterial activity, and the new

antibiotic-modified Ti holds great potential for dental/bone implant in clinic.

2. Material and methods

2.1. Materials

Commercial pure titanium (Ti), grade 2, was purchased from Northwest Institute for Non-ferrous Metal Research (Xi'an, China). Dopamine was purchased from Sigma-Aldrich Chemical Co. (MO, USA), and tris[hydroxymethyl]aminomethane (Tris) was supplied from Aladdin Reagent Co., Ltd (Shanghai, China). CS ($C_{16}H_{16}N_5O_7S_2Na$) was provided by Amresco Inc. (OH, USA). All other chemicals were of analytical reagent grade and were used as received unless noted. All aqueous solutions were prepared with de-ionized water (DI water).

2.2. Immobilization of cefotaxime sodium on the surface of titanium

To prepare CS-decorated Ti with antibacterial activity, Ti substrates were pre-modified with pDA coating, and CS was subsequently immobilized onto the surface of pDA-modified Ti substrates as shown in figure 1. In brief, prior to surface modification, Ti substrates were cut into discs of 15 mm in diameter and 2 mm thick. These substrates were polished with a series of SiC abrasive papers (400, 1000, 1500, 2000 grit), cleaned ultrasonically for 20 min in baths of acetone, anhydrous ethanol and DI water, respectively, and then dried at 50°C overnight. pDA was anchored to the surface of Ti discs as described elsewhere [27,28], via immersion of the substrates in a 2 mg ml^{-1} solution of dopamine (10 mM Tris–HCl buffer, pH = 8.5), and gently shaken overnight in the dark. After this process, these Ti substrates were then rinsed with DI water to remove the unattached dopamine molecules and dried in a stream of nitrogen. Subsequently, the pDA-grafted Ti substrates were treated with CS in 50 mg ml^{-1} concentration dissolved in 10 mM Tris buffer (pH = 8.5), and incubated with stirring overnight at room temperature. CS was grafted onto the pDA-coated Ti via reaction between the amino groups in CS and the catechol/quinone groups in pDA through Michael addition and Schiff-base reactions. The possible chemical structure is also shown in figure 1. The antibiotic-decorated Ti discs were then washed three times with DI water to remove unattached CS molecules and left to air dry before use. The substrates are denoted Ti (pristine pure titanium), Ti-pDA (polydopamine-coated Ti) and Ti-pDA-CS (cefotaxime sodium-decorated, polydopamine-coated Ti) in subsequent discussions. The prepared CS-decorated Ti interfaces were subjected to tests as described below.

2.3. Surface characterization

2.3.1. Contact angle measurements

Contact angles on the pristine and decorated Ti were measured at room temperature by the sessile drop method using 2 µl DI water droplet in a contact angle measuring device (SL200B, Kono, USA). Additionally, the advancing and receding water contact angles were measured. Six samples in each stage were used to provide an average and standard deviation.

2.3.2. X-ray photoelectron spectroscopy

X-ray photoelectron spectroscopy (XPS, AXIS Ultra, Kratos Analytical Ltd, Japan) was used to identify the chemical constituents and elemental states of the different prepared Ti samples. The binding energies were calibrated by the C 1s hydrocarbon peak at about 285 eV and by the N 1s peak at about 400 eV.
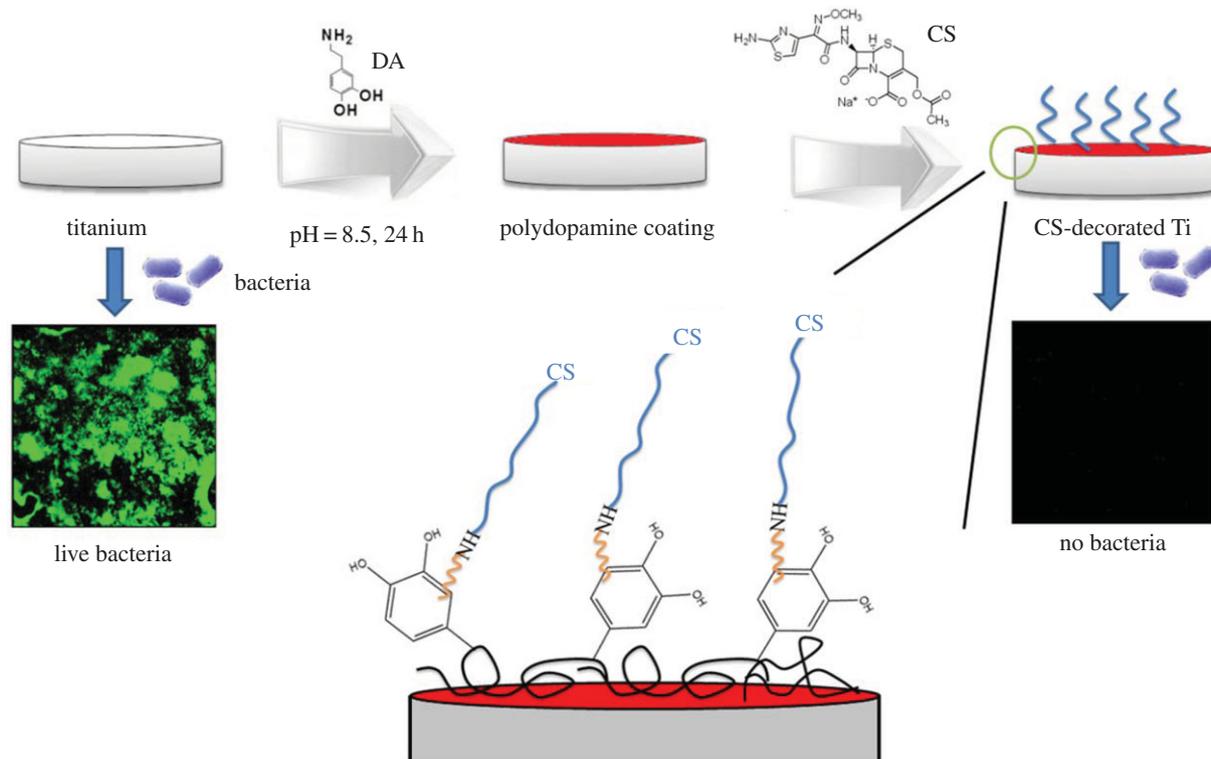
Figure 1. Schematic of preparation of cefotaxime sodium-decorated Ti through pDA coating and its antibacterial activity assay. The possible chemical structure as well as the suggested reaction mechanism are also shown. (Online version in colour.)

The quantitative analysis and the curve fitting were conducted using the CASAXPS software package.

2.3.3. Scanning electron microscope

The morphology of the unmodified and modified Ti substrates was characterized by using a field-emission scanning electron microscope (FE-SEM, JSM-6701F, JEOL, Tokyo, Japan). All samples were coated by gold for 1 min before SEM observation.

2.3.4. Atomic force microscope

Atomic force microscope (AFM, PI3800/SPA400, Seiko Instruments, Japan) was used in tapping mode (15 μm scanner) in dry condition at ambient temperature to assess morphological characteristics of Ti substrates treated by pDA and CS solutions. Surface roughness (Ra) was also calculated from the roughness profile. Each sample was tested in triplicate to the arithmetic average. For the tapping mode measurement, we used a Si_3N_4 cantilever with a spring constant of 0.12 N m^{-1} (Seiko Instruments) for resolution imaging. The scan range was 20×20 μm, and scan rate was 1 Hz. Before AFM measurement, the different Ti substrates were rinsed with ethanol and DI water, and allowed to air dry.

2.4. In vitro cytotoxicity

2.4.1. Cell culture

Human osteoblast-like MG-63 cells (American Type Culture Collection, VA, USA) were cultured in Dulbecco's modified Eagle's medium (DMEM, Gibco, Carlsbad, CA) containing 10% fetal calf serum (Gibco), 100 μg ml^{-1} streptomycin (Amresco, Cleveland, OH, USA) and 100 μg ml^{-1} penicillin (Amresco) at 37°C in a humidified atmosphere of 5% CO_2.

2.4.2. Cell viability assay

The in vitro cytotoxicity of MG-63 cells was assessed using the cell counting kit-8 assay (CCK-8, Dojindo, Japan). After cell counting, MG-63 cells were seeded in 24-well plates (Costar, USA) at a density of 1×10^5 cells per well. After seeding for 24 h, cells were rinsed with phosphate-buffered saline (PBS) buffer, and exposed to the pristine and CS-decorated Ti interfaces. The control groups involved the use of DMEM as negative control and 10% dimethylsulfoxide DMEM as positive control. After incubating for 1, 3, 5 days, respectively, CCK-8 was added into each well for 4 h incubation, then supernatant was transferred to new 96-well cell culture plates. The absorbance value of supernatant optical density (OD) was measured with a microplate reader (model 680, Bio-Rad, CA) at 450 nm wavelength, with a reference wavelength of 630 nm. The cell viability was expressed as a percentage as follows:

$$\text{Cell viability} = \frac{\text{OD (test)} - \text{OD(blank)}}{\text{OD(negative control)} - \text{OD(blank)}} \times 100\%.$$

2.4.3. Field-emission scanning electron microscope observation of cells

The typical cellular attachment and spread morphologies on the pristine and decorated Ti were evaluated by FE-SEM after Au sputtering. Basically, after 1, 3 and 5 days incubation under the culturing condition mentioned above, the samples with cells were rinsed in PBS buffer and in 2.5% glutaraldehyde solution for 1 h, followed by dehydration with graded ethanol solutions and dried.

2.5. Haemocompatibility assessment

2.5.1. Haemolysis tests

Healthy human blood from volunteers containing sodium citrate (3.8 wt%) in the ratio of 9 : 1 was taken and diluted with normal saline (4 : 5 ratio by volume). The pristine Ti and CS-decorated Ti interfaces were dipped in a standard tube containing 10 ml of normal saline that were previously incubated at 37°C for 30 min. Then, 0.2 ml of diluted blood was added to this standard tube, and the mixtures were incubated for 60 min at 37°C. Similarly, normal saline solution was used as a negative control, and

DI water as a positive control. After the incubation, all the tubes were centrifuged for 5 min at 3000 rpm, and the supernatant was carefully removed and transferred to a new 96-well plate for spectroscopic analysis by a microplate reader (model 680, Bio-Rad, CA) at 545 nm. In addition, the haemolysis was calculated based on the average of three replicates:

$$\text{Haemolysis} = \frac{\text{OD(test)} - \text{OD(negative control)}}{\text{OD(positive control)} - \text{OD(negative control)}} \times 100\%.$$

2.5.2. Platelet adhesion

Platelet-rich plasma (PRP) was prepared by centrifuging the whole blood for 10 min at a rate of 1000 r.p.m. The PRP was overlaid atop the decorated Ti plates and incubated at 37°C for 1 h. After incubating, all samples were rinsed with PBS buffer three times to remove the non-adherent platelets. The adhered platelets were also fixed in 2.5% glutaraldehyde solutions for 1 h at room temperature followed by dehydration in a gradient ethanol/distilled water mixture (from 25% to 100%) for 15 min each and dried. The interface of platelets attached to the decorated Ti sheets was observed by FE-SEM.

2.6. *In vitro* antibacterial activity assay

In this work, a semi-quantitative measurement of bacterial adhesion on the pristine and decorated Ti was performed via microbial viability assay kit-WST. *Escherichia coli* (*E. coli* 1.1369, obtained from China General Microbiological Culture Collection Center, PR China) and *Streptococcus mutans* (*S. mutans* UA159, obtained from American Type Culture Collection, USA) were cultivated in Luria–Bertani (LB) medium (containing 10 g l^{-1} peptone, 5 g l^{-1} yeast extract and 10 g l^{-1} sodium chloride) and brain heart infusion medium (containing 10 g l^{-1} proteose peptone, 2 g l^{-1} dextrose, 5 g l^{-1} sodium chloride and 2.5 g l^{-1} disodium phosphate), respectively. After an overnight culture at 37°C, respective colony-forming unit (CFU) counts were determined from the absorbance at 600 nm wavelength using previously established standard curves. The concentrations of *E. coli* and *S. mutans* in broth were adjusted to give an initial OD reading of 0.200 and 0.175 at the wavelength of 600 nm, which corresponded to a concentration of 1×10^6 CFU ml^{-1}. Cells were then centrifuged at 10 000 r.p.m. at 4°C (5804R centrifuge, Eppendorf, Germany), and the pellets re-suspended in sterile saline solution. For the bacterial attachment and proliferation assay, the pristine and antibiotic-decorated Ti were sterilized under UV irradiation for 30 min each side, then placed in a 24-well tissue plate (Corning, USA) and covered with two different 40 μl bacterial solutions with about 10^6 CFU ml^{-1} of the desired strain and 760 μl prepared medium for 4 h–28 days. All samples were kept in an incubator containing 5% CO$_2$ for desired time at 37°C. Meanwhile, the minimum bactericidal concentration of CS solution (32 mg ml^{-1}) was added into the above mixture of bacterial solution and culture medium as the control. The medium was changed every 24 h. At scheduled times, substrates were taken out, gently rinsed with PBS three times to remove non-attached bacteria, and placed into new 24-well tissue plate and incubated with 20 μl WST, which produced a water-soluble formazan dye upon reduction by dehydrogenase in cells, and 380 μl medium for another 2 h. Then, OD value ($\lambda = 450$ nm) of the suspension in each well was measured on a microplate reader (Elx808, Bio-Tek, USA).

2.7. Field-emission scanning electron microscope observation of bacteria cells

Bacterial solution of two different bacteria (20 μl) and 2 ml prepared medium were cultured on the pristine and CS-decorated Ti interfaces. The morphologies and numbers of *E. coli* or *S. mutans* bacteria cultured with the different Ti interfaces were
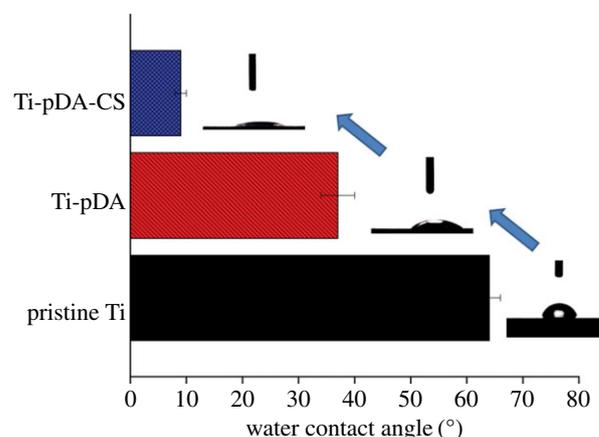
Figure 2. Water contact angle and representative images of water droplet on different Ti sample surfaces. (Online version in colour.)

observed using FE-SEM after 24 h culture. All samples were fixed in 2.5% glutaraldehyde solution in PBS for 30 min and then dehydrated with a series of graded ethanol solutions for SEM testing. Dehydrated samples were dried by a vacuum dryer before sputter-coating with gold using a sputter coater. The number of adherent bacteria was counted at the projected area (magnification 100×), obtained from five different areas (up, down, left, right and centre) per sample ($n = 3$).

2.8. *In vitro* anti-biofilm formation assay

Biofilm formation on the interface of the CS-decorated Ti was probed using a confocal laser scanning microscope (CLSM). A LIVE/DEAD BacLight bacterial viability kit (L-7007, Invitrogen, USA) was used to determine the long-term bacterial cell viability on the interfaces. In this assay, the red-fluorescent nucleic acid staining agent propidium iodide, which penetrates only damaged cell membranes, was used to label dead bacterial cells. By contrast, the SYTO9 green-fluorescent nucleic acid staining agent, which can penetrate cells with both intact and damaged membranes, was used to label all the bacterial cells. The bacteria (20 μl bacterial solution and 2 ml prepared medium) were seeded onto the pristine and CS-decorated Ti interfaces followed by incubation at 37°C for 7 days. The supernatant was removed, and the substrates were washed with PBS buffer at least three times. They were then incubated in a 24-well plate with 400 ml of a dye-containing solution, which was prepared by adding 6 μl of SYTO (3.34 mM) and 6 μl of propidium iodide (20 mM) to 4 ml of PBS buffer at room temperature in the dark for 15 min, according to the manufacturer's protocol. The stained bacterial cells were examined under a Zeiss LSM510 laser scanning confocal microscope (Germany). Images were obtained using an oil immersed 40× object lens under the same conditions.

2.9. Statistical analysis

All data were expressed as mean standard deviations of a representative three similar experiments carried out in triplicate. Statistical analysis was performed with ORIGIN software. Student's *t*-test was used to determine the significant differences among the groups, and *p*-values less than 0.05 were considered statistically significant.

3. Results and discussion

3.1. Surface wettability analysis

Water contact angle on a substrate can provide information on wettability and surface energy of the substrate and has
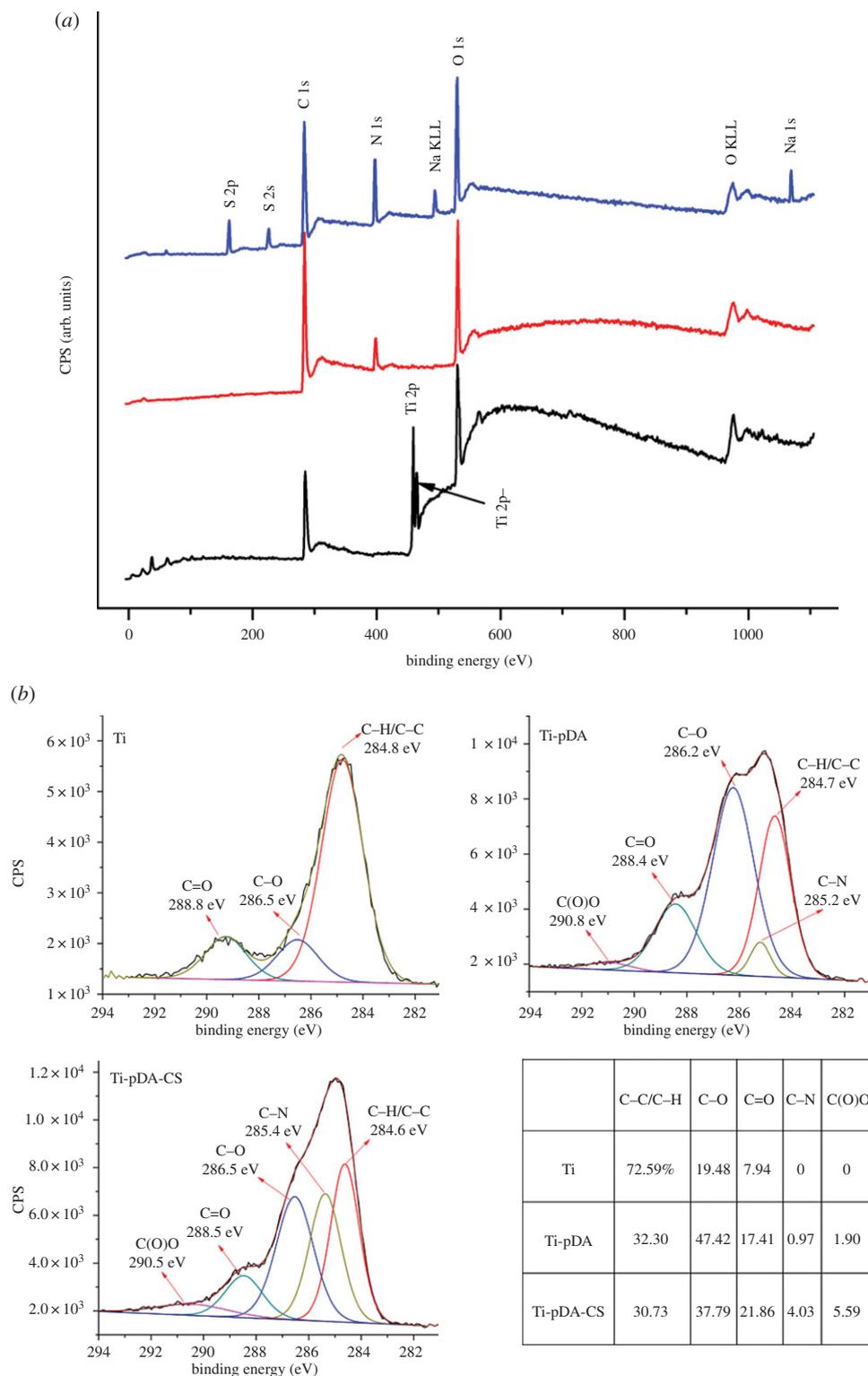
Figure 3. XPS survey scan spectra: (*a*) XPS wide spectra of the pristine Ti, Ti-pDA and Ti-pDA-CS; (*b*) high-resolution spectra of carbon peaks (C 1s) for the pristine Ti, Ti-pDA and Ti-pDA-CS, and the relative of content functional groups. (Online version in colour.)

	C–C/C–H	C–O	C=O	C–N	C(O)O
Ti	72.59%	19.48	7.94	0	0
Ti-pDA	32.30	47.42	17.41	0.97	1.90
Ti-pDA-CS	30.73	37.79	21.86	4.03	5.59

been widely used to track and evaluate effectiveness of surface modification protocols. The surface wettability of pDA-coated substrates has been well documented previously. For example, the water contact angle of clean glass $(11 \pm 1°)$ increased to $44 \pm 2°$ after 24 h of pDA coating, and pDA-coated polyvinylidene fluoride film showed a dramatic decrease in water contact angle [29]. In good agreement with previous reports, the water contact angle on Ti substrates coated with pDA significantly decreased from $64 \pm 2°$ to $37 \pm 3°$. In addition, immobilization of antibiotic on the pDA-coated Ti surface sharply decreased the water contact angle to $9 \pm 1°$, attributed to super-hydrophilicity of CS, which implied that the antibiotic CS was successfully grafted to the Ti surface. The representative water droplet images are depicted in figure 2.

3.2. Chemical constituent characterization

To verify the results obtained from the surface wettability assessment, XPS was used to provide direct evidence of the detailed chemical composition on the functionalized Ti. The XPS survey spectra and quantitative XPS analysis results are
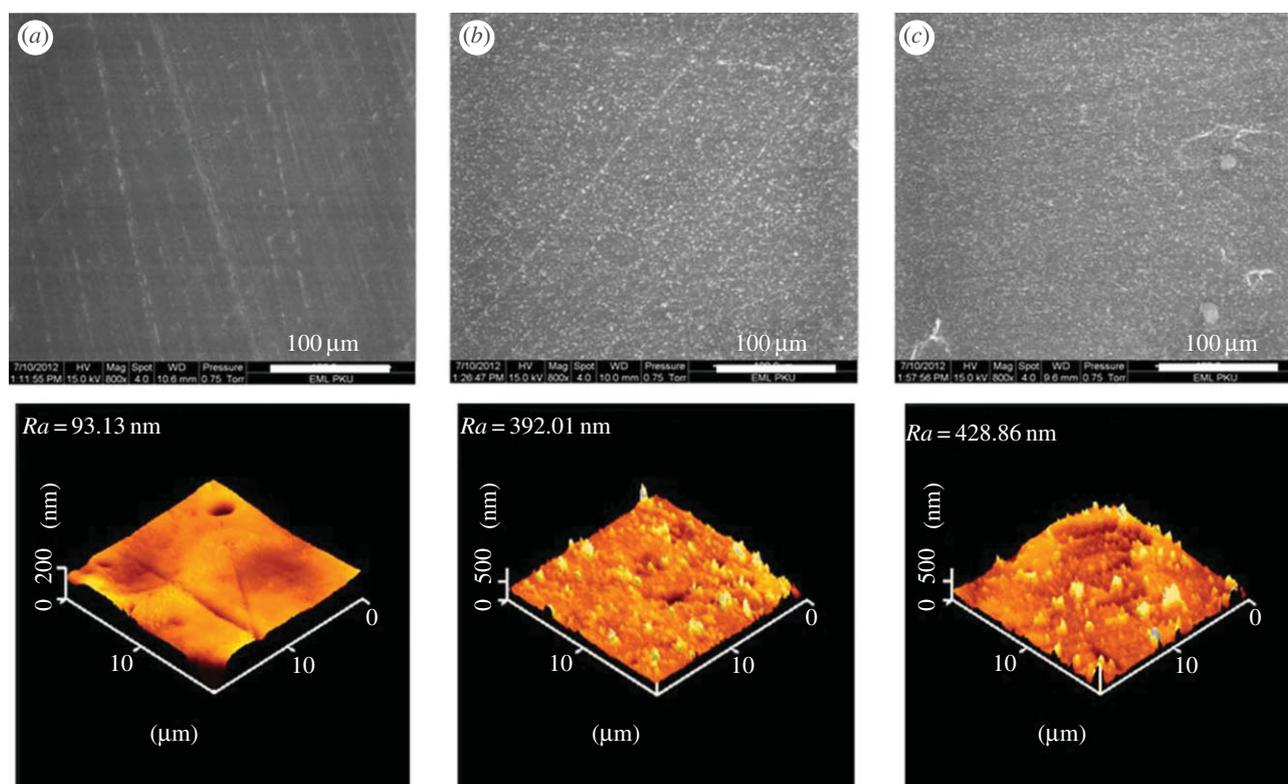
Figure 4. SEM and corresponding AFM images of the (*a*) pristine Ti, (*b*) pDA-coated Ti and (*c*) CS-decorated Ti samples. (Online version in colour.)

Table 1. Elemental composition of the pristine Ti, pDA-coated Ti and CS-decorated Ti determined by XPS analysis.

elements	pristine Ti (%)	Ti-pDA (%)	Ti-pDA-CS (%)
C 1s	9.69	73.34	58.91
O 1s	38.04	17.42	20.18
Ti 2p	52.27	0.22	0
N 1s	0	9.02	14.26
S 2p	0	0	4.88
Na 1s	0	0	1.78

shown in figure 3 and the electronic supplementary material, figures S1–S2 and table 1. The pristine Ti showed strong Ti 2p, Ti 2p- and O 1s peaks as well as C 1s (figure 3*a*). Carbon, typically present from unavoidable hydrocarbon con-tamination, was used as an internal reference at 284.6 eV for calibrating peak positions [30]. Successful deposition of pDA on the Ti substrate was indicated by an increase in the N and C contents as shown in table 1. Nitrogen-to-carbon (N/C) ratio was about 0.123 on Ti-pDA which was similar to the theoretical N/C of 0.125 for dopamine [31]. Further-more, complete suppression of photoelectron peaks unique to Ti 2p confirmed formation of the pDA thin film. Upon attachment of CS on Ti-pDA, notably in the wide-scan spectra, the appearance of sulfur signal (S 2s and S 2p; the electronic supplementary material, figure S1) and sodium signal (Na 1s and Na KLL), and the enhancement of nitrogen peaks (N 1s) on the surface of Ti-pDA-CS indicated successful immobiliz-ation of the antibiotic. Furthermore, an evident change in carbon bond composition observed in the high-resolution narrow carbon spectra (C 1s) clearly supported these

conclusions (figure 3*b*). The high-resolution C 1s spectrum of the pristine Ti was deconvoluted into three different curves. The binding energies centred at 284.8, 286.5 and 288.8 eV were assigned to the carbon skeleton (–C–C–/–C–H–), hydroxyl group (–C–OH) and carbonyl group (–C=O), respectively [32,33]. A broad peak assigned to the –C–N– bond at about 285 eV was recorded on both Ti-pDA and Ti-pDA-CS samples, indicating the presence of pDA and CS. Additionally, after pDA coating, the intensity of the carbon skeleton (–C–C–/–C–H–) peak decreased dramatically, and the peaks of the hydroxyl and carbonyl groups increased as shown in figure 3*b*. They should be attributed to the catechol/quinone groups of pDA. Compared with those of the Ti-pDA, the peaks of the –C=O, –C(O)O– and especially –C–N– for the Ti-pDA-CS increased greatly in intensity owing to abundant amide bond (–NH–C=O) in the structure of CS molecules. Moreover, in the high-resolution N 1s spectra of pDA-coated and CS-decorated Ti surface (the electronic supplementary material, figure S2), a peak at about 399.9 eV, which is related to the –CO–NH– bond, was found. In the spectrum of CS-decorated Ti surface, how-ever, a new peak at 401.8 eV was observed, which might correspond to another nitrogen state in CS, further proving the successful CS coating. These results obviously suggested that CS was immobilized on the pDA-coated Ti. Antibacterial copo-lymers (containing poly(ethylene glycol) (PEG)-based polymers and quaternary ammonium-based polymers) [1,12,14,15,30,34] and silver ion [34] were immobilized onto Ti implants using pDA coating in previous studies by other groups and some pro-spective results were achieved. For example, thiol-terminated methoxy-PEG was used to graft onto pDA-coated substrates, and these modified surfaces exhibited antifouling property against bacterial and mammalian cells [1,27]. PEG or PEG-based coatings, as a passive strategy, have been of great interest in the drive to develop antifouling surfaces, which rely on
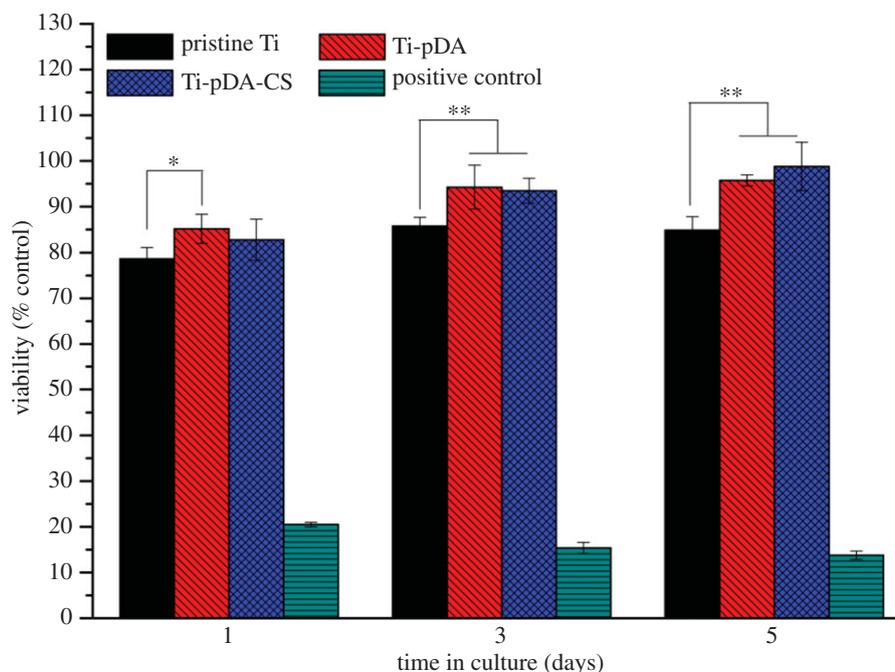
Figure 5. The cell proliferation rates of MG-63 cell lines cultured in the media for 1, 3 and 5 days with different Ti samples. Asterisks indicate significance level obtained by t-test: $*p < 0.05$; $**p < 0.01$. (Online version in colour.)

Table 2. Advancing and receding water contact angles and hysteresis of the pristine Ti, pDA-coated Ti and CS-decorated Ti samples.

materials	advancing angle (°)	receding angle (°)	hysteresis (°)	Ra (nm)
pristine Ti	65 ± 7	54 ± 3	11 ± 5	93.13
Ti-pDA	48 ± 6	28 ± 2	20 ± 3	392.01
Ti-pDA-CS	22 ± 2	0 ± 0	22 ± 2	428.86

physical prevention of bacteria and cell attachment rather than eradicating bacteria [12]. Therefore, PEG-based polymer surfaces do not display good biocompability owing to inhibition of cell attachment. Moreover, decreased antifouling performance of PEG coatings over time is a major issue [14]. Quaternary ammonium-based polymers, biocides, are typically more potent against Gram-positive bacteria such as *S. aureus* and are less active against Gram-negative bacteria such as *E. coli* [15,35]. As for silver ion, extensive silver nanoparticles cause many severe side effects, such as cytotoxicity and internal organ injury [36,37]. They all face a major challenge in terms of promoting antibacterial properties. Therefore, the development of a novel Ti implant with enhanced antibacterial activity through a green, facile and effective implant modification method is crucial and in great demand.

3.3. Surface morphology and roughness

Ti substrates with immobilized pDA and antibiotic were analysed by AFM and SEM to investigate surface morphology and roughness. The unmodified Ti exhibited smooth surface morphology, compared with the modified substrates (figure 4a). Dopamine is known to be polymerized under slightly alkaline conditions (pH 8.5), and polymerized dopamine can be spontaneously deposited onto many types of substrates, including metals and polymers [38,39]. As shown in figure 4, SEM and AFM investigations revealed the difference in the surface morphology between Ti, Ti-pDA and Ti-pDA-CS

samples. After pDA coating, partial aggregates of polymerized dopamine were found, which confirmed the pDA layer on the Ti surface (figure 4b). In previous work, homogeneous deposition of pDA was achieved in the range of few minutes to 24 h that covered throughout the surface of substrates [27,28]. As the coating time increased, pDA layer seemed to be thickened by multiple depositions of pDA layers. During prolonged coating process, we observed that polymerized dopamine changed surface morphology (appearance of nano-sized aggregates or lumps). Moreover, the surface roughness was determined by AFM. Following dopamine modification, the relative roughness of Ti-pDA increased by about 427% compared with the pristine Ti to average 392.01 nm. Addition of CS slightly increased the surface roughness of the Ti-pDA substrates. Contact angle hysteresis generally correlates with the roughness of the surface [40,41]. Data in table 2 clearly show significantly higher contact angle hysteresis in pDA-coated Ti surfaces versus pristine Ti control surface, which also suggests significant increase in surface roughness owing to pDA coating. Only slightly higher hysteresis was detected after immobilization of CS. These results are consistent with SEM and AFM analyses.

3.4. *In vitro* cytotoxicity evaluation

The cytotoxicity of the as-prepared antibiotic-decorated Ti to human osteoblast-like MG-63 cells is another important factor that should be carefully evaluated when the novel
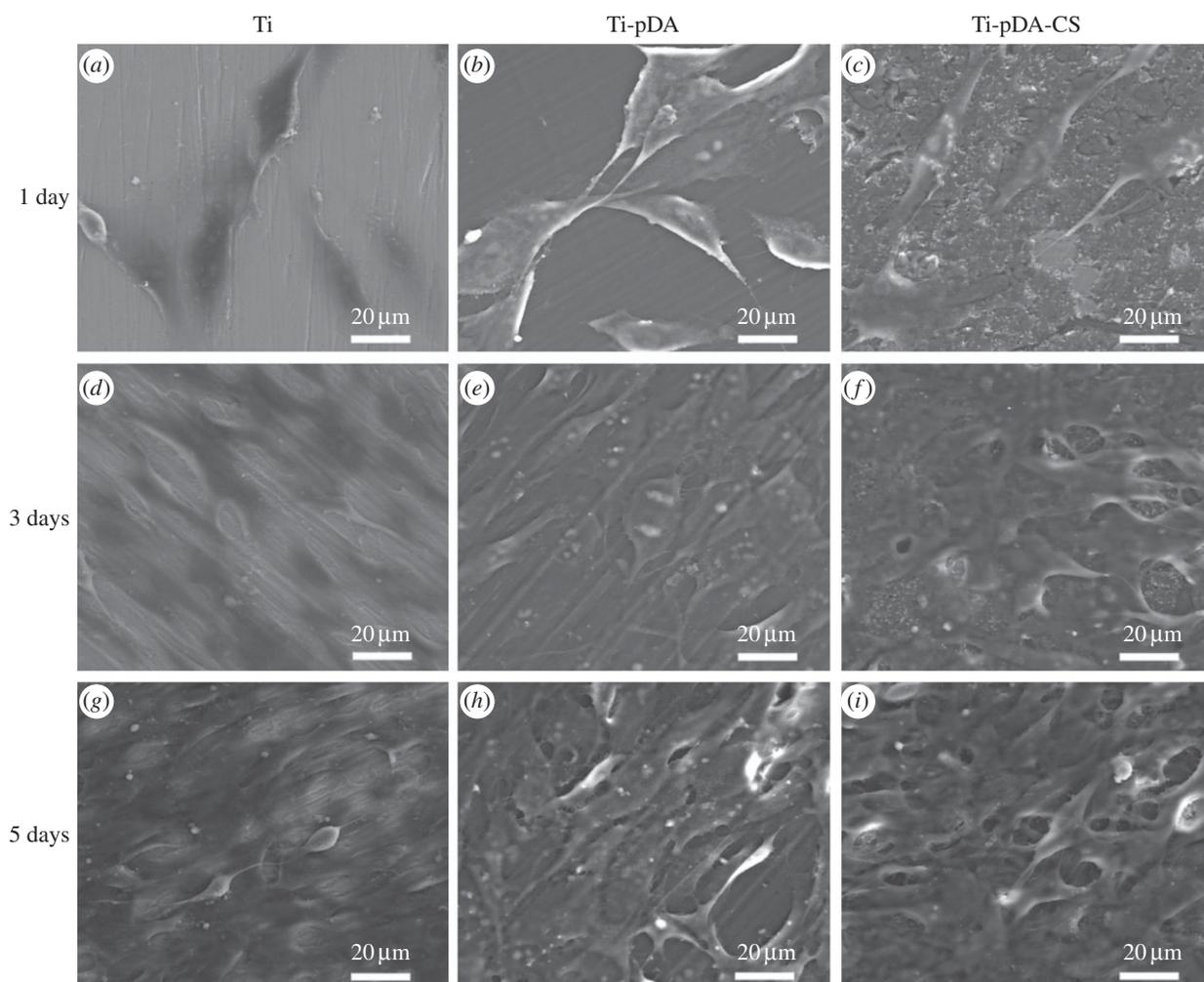
Figure 6. The MG-63 cell morphologies on the (*a, d* and *g*) pristine Ti, (*b, e* and *h*) Ti-pDA and (*c, f* and *i*) Ti- pDA-CS interfaces after 1, 3 and 5 days cell culture.

antibiotic-decorated Ti is used in biological and biomedical applications, such as dental/bone implant. Figure 5 shows the *in vitro* MG-63 cell viability cultured with the pristine and CS-decorated Ti samples in DMEM for 1, 3 and 5 days, assessed by CCK-8 assay. The viability value increased with time when MG-63 cells were co-cultured with the decorated Ti surface, indicating that functionalization of Ti surface had affected cell proliferation. The viability of cells on Ti-pDA samples for 1 day displayed little statistical differences to the pristine Ti group. However, after incubating for 3 and 5 days, Ti-pDA and Ti-pDA-CS groups displayed higher cell viability than that of the pristine Ti counterparts, even though cells cultured with Ti-pDA and Ti-pDA-CS samples showed no statistical differences in cell viability. These results indicated that the pDA-modified Ti substrates kept a better viability all the time, and that the adhesion of pDA might have a positive influence on the cytocompatibility of the Ti, which was consistent with other previous researches [23,28]. CS-decorated Ti samples also exhibited the best cytocompatibility among all samples on the fifth day. Thus, it could be concluded that the adhesion of antibiotic CS on the Ti substrate surfaces would present excellent cytocompatibility and better cell viability than the pristine Ti and that CS-grafted Ti implant has great potential for hard tissue replacement and other biological and biomedical applications.

A typical overview of MG-63 cell morphologies on the pristine Ti and different functionalized Ti samples for 1, 3 and 5 days is shown in figure 6. The number of cells attached on each sample increased with the extension of culture time, and MG-63 cells were adhered onto the surfaces and spread pseudopodia to form cell layers on the surfaces at 5 days. Previous reports demonstrated that pDA coating could enhance adhesion and survival of the cells [42,43] and promote osteogenic differentiation [44]. Compared with that on Ti, higher amount of cells could be observed on Ti-pDA and Ti-pDA-CS. On the interfaces of the Ti-pDA-CS substrates, the cells had healthy spindle shapes, spread with ruffling of peripheral cytoplasm, covered almost the whole surfaces, and flattened with a larger attachment area compared with the cells cultured on the pristine Ti interface, in accordance with CCK-8 results. These observations and results confirm that the adhesion of the pDA and CS on the Ti interfaces could promote cell attachment and growth, and greatly improve the biological activity of the grafted Ti implant.

3.5. Haemocompatibility evaluation

Figure 7*b* shows the morphologies of human platelets adhering to the pristine Ti and CS-decorated Ti samples after incubation in PRP for 1 h. The number of adhered platelets seemed to be similar for the two different Ti groups, though the shape and activation status of the platelets behaved in a different way. From the enlarged images of
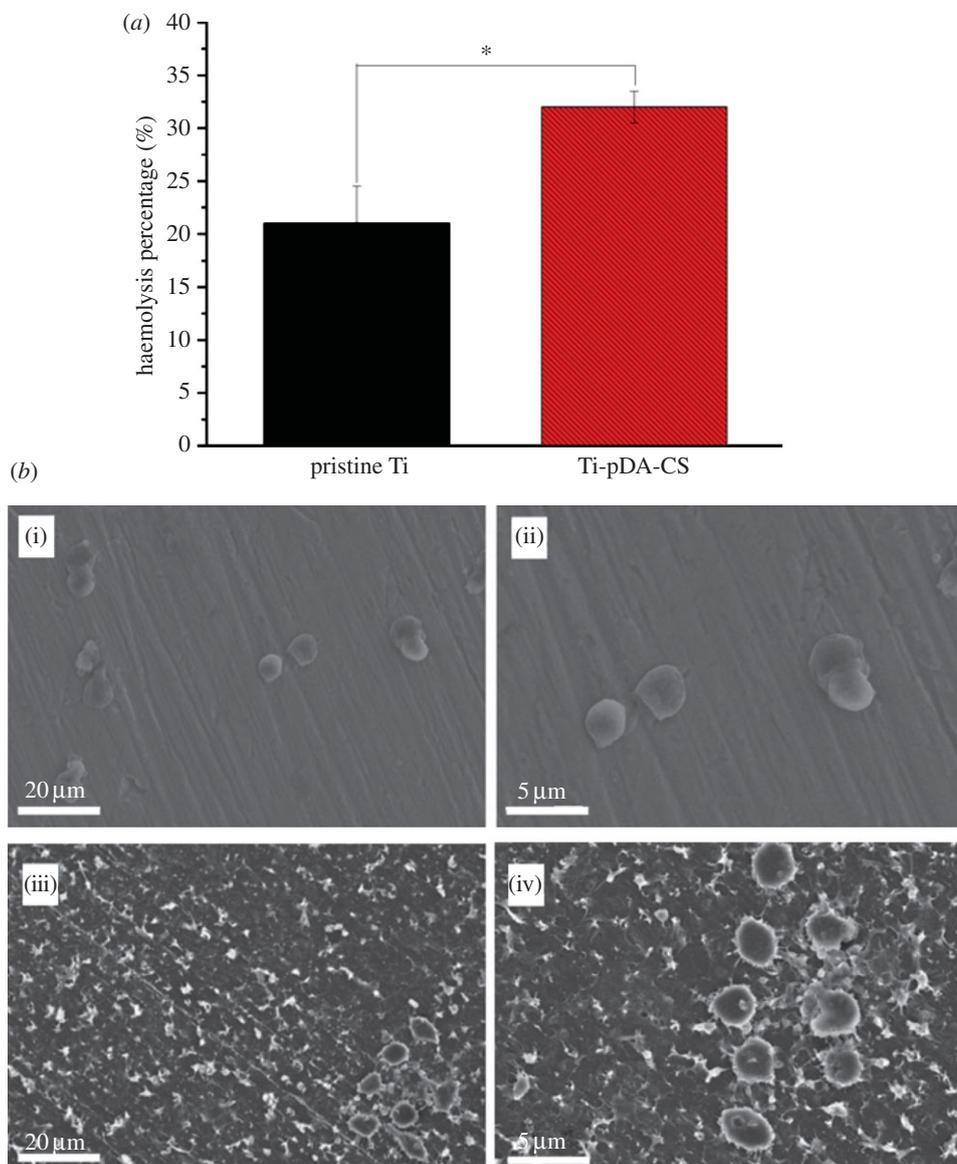
Figure 7. Haemocompatibility assessment of (a) haemolysis rate; (b) the SEM observation of adhered platelets on the interfaces of the pristine Ti (b(i)(ii)) and CS-decorated Ti (b(iii)(iv)). Asterisk indicates significance level obtained by t-test: *$p < 0.05$. (Online version in colour.)

CS-grafted Ti groups, it could be seen that a cluster of positive platelets with short pseudopodia were scattered (figure 7b(iii)(iv)), and higher haemolysis was detected on the CS-decorated Ti interfaces (figure 7a). On the other hand, round- and smooth-shaped platelets were observed on the interface of the pristine Ti groups. This might be ascribed to the increase of surface roughness of the Ti-based substrates after pDA coating, which was confirmed from SEM and AFM images. The enhancement of surface roughness is proved to lead to higher haemolysis ratio and activation of platelets [45]. However, it was noteworthy that the haemolysis rates for both the pristine Ti and CS-grafted Ti samples stayed much lower than 5%, which is regarded as a biosafety threshold and represents well-behaved haemocompatibility as illustrated in figure 7a.

3.6. Antifouling and antibacterial activities

The initial adhesion of bacteria to implant interfaces is the initial and crucial step for biofilm formation, which plays an imperative role in the pathogenesis of infection [46]. The prevention of bacterial adhesion to implanted biomaterials, such as Ti implants, during the early post-implantation period is vital to the efficacy and long-term success of an implant. The investigation of initial bacterial adhesion was carried out on the substrates incubated for 4 h, which was deemed sufficient to reflect the bacterial contact in the early 'decisive period' of implant infection [47]. The semi-quantification of viable bacterial cells on the interfaces of the substrates was done via microbial viability assay kit. In order to assess the wide range of antibacterial activity of the CS-decorated Ti interfaces, both Gram-negative E. coli, the most common bacteria in implant infection, and Gram-positive S. mutans, one of the early colonized bacteria in oral biofilm and the major pathogen responsible for dental caries in humans [48], were selected as the experimental strains. Figure 8 shows the amount of viable E. coli and S. mutans cells adhered on the pristine Ti, Ti-pDA and Ti-pDA-CS interfaces at 4, 24 and 72 h. The minimum bactericidal concentration of the CS solution (32 mg ml^{-1}) as the control was added into the above mixture of two bacterial solutions and culture medium. At the stage of the initial adhesion, compared with the pristine Ti, few bacterial cells were detected on the CS-decorated Ti interface for
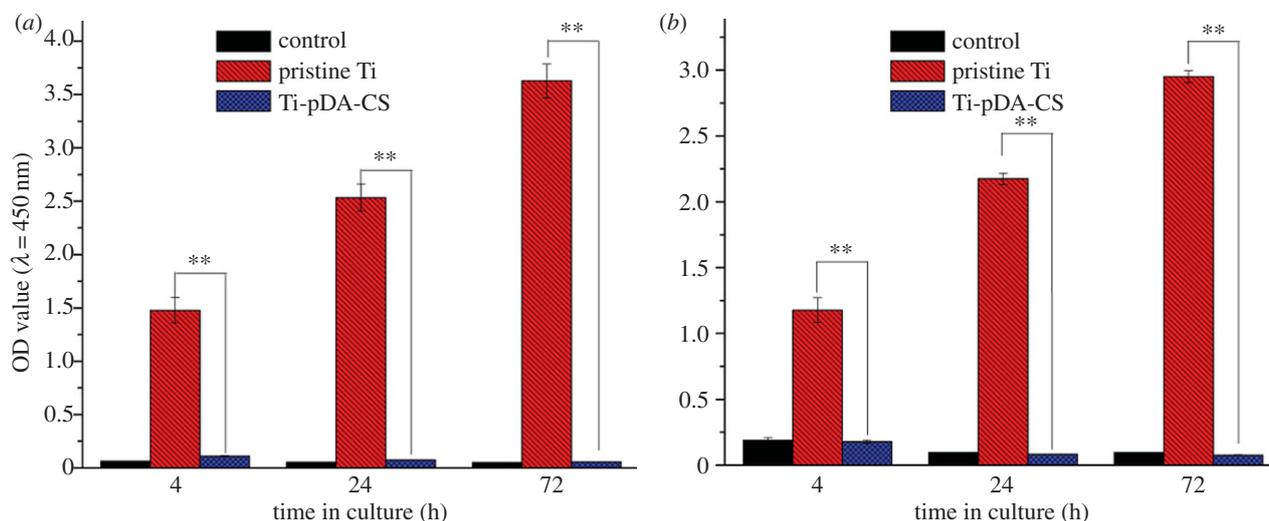
Figure 8. Antifouling and antibacterial activities of the pristine Ti and CS-decorated Ti samples against (*a*) *E. coli* and (*b*) *S. mutans* bacteria cultured for 4, 24 and 72 h. The minimum bactericidal concentration of CS solution (32 mg ml^{-1}) was added into the mixture of bacterial solution and culture medium as the control group. Asterisks indicate significance level obtained by *t*-test: **$p < 0.01$. (Online version in colour.)
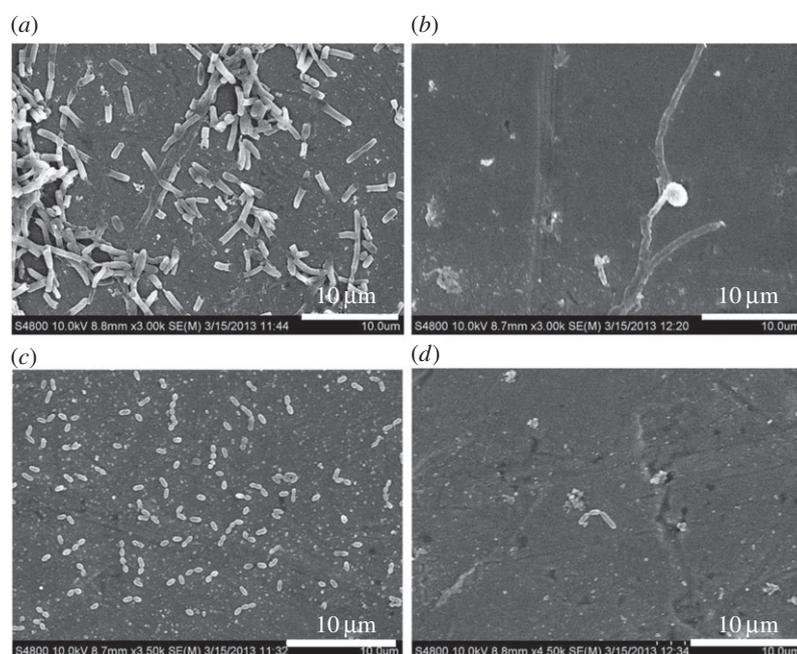

Figure 9. SEM images of the morphology and number of adherent *E. coli* and *S. mutans* after incubation with the pristine Ti and CS-grafted Ti interfaces: (*a*) the pristine Ti with *E. coli*, (*b*) the Ti-pDA-CS with *E. coli*, (*c*) the pristine Ti with *S. mutans* and (*d*) the Ti-pDA-CS with *S. mutans*.

both bacteria, demonstrating good antifouling properties of the CS-decorated Ti. At the proliferation stage, the OD value increased with time when two different bacteria were cultured on the pristine Ti interface (figure 8), indicating that pristine Ti implants were prone to bacterial cell proliferation and subsequent infection. However, for both bacteria, there was a clear reduction in the number of adherent cells on the Ti-pDA-CS interfaces. For instance, at 24 h in contact with *E. coli* the Ti-pDA-CS modified substrates showed more than 97% reduction in bacterial adhesion compared with the pristine Ti. In the case of *S. mutans*, the Ti-pDA-CS substrates demonstrated similar efficacy (about 96%) in reducing the number of adherent bacteria. More importantly, the number of *E. coli* and *S. mutans* on the CS-decorated Ti interfaces did not increase as time went on, which was significantly different from that of the pristine Ti. Moreover, there were no differences in the number of adherent *E. coli* and *S. mutans* between Ti-pDA-CS group and control group at

each time point, which demonstrated that the CS-decorated Ti interface significantly inhibited bacterial adhesion and proliferation.

To verify the results obtained from the microbial viability analysis, SEM was applied to observe the morphology and number of bacterial cells on the pristine Ti and CS-decorated Ti interfaces. As shown in figure 9, *E. coli* displays rhabditi form morphology, whereas *S. mutans* displays typical coccal or ellipsoid form. A great number of both *E. coli* and *S. mutans* cells were found on the pristine Ti interface after 24 h bacterial culture. Compared with the pristine Ti, only a small number of bacterial cells were observed on the CS-grafted Ti interface, in accord with the results from the microbial viability analysis. Additionally, the number of adherent cells counted from SEM on the Ti-pDA-CS samples was significantly less than that on the pristine Ti ones (the electronic supplementary material, figure S3). Our results indicate that CS antibiotic retains its biological activity
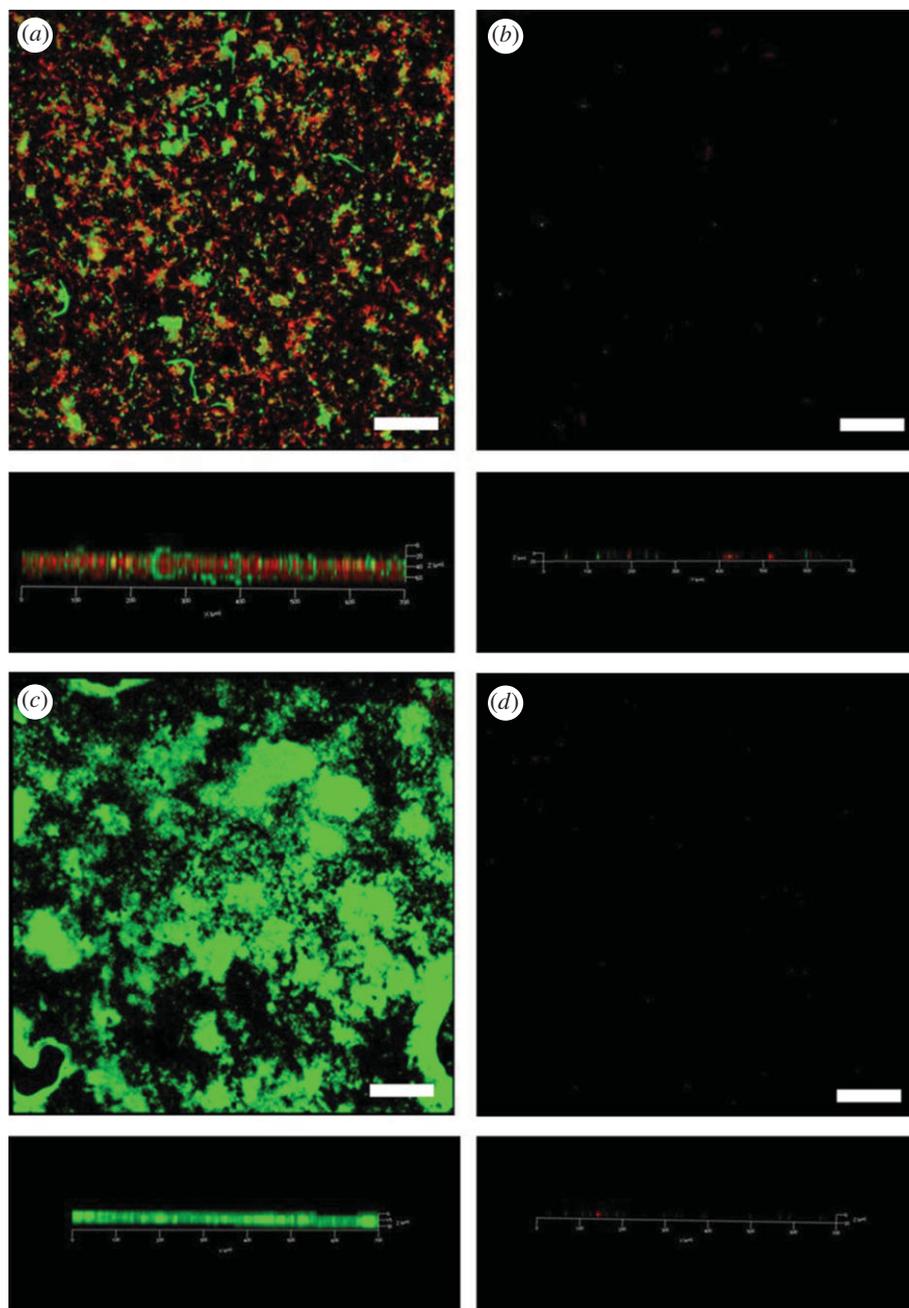
Figure 10. Live/dead cell staining on the pristine and CS-grafted Ti interfaces after 7 days of incubation with *E. coli* and *S. mutans*: (*a*) the pristine Ti with *E. coli*, (*b*) the Ti-pDA-CS with *E. coli*, (*c*) the pristine Ti with *S. mutans* and (*d*) the Ti-pDA-CS with *S. mutans*. Scale bar, 10 μm. (Online version in colour.)

after being immobilized onto the surface of Ti-pDA and exhibits excellent *in vitro* antibacterial activity no matter whether Gram-negative or Gram-positive bacteria.

3.7. Prevention of biofilm formation

Following initial bacterial attachment onto the implant–abutment interface, there is a prolonged accumulation phase involving cell proliferation and intercellular interaction followed by biofilm formation. Biofilm formed on surfaces consists of bacteria, their secretion and extracellular polymeric substances (EPS) [49]. EPS produced by biofilms can act as a barrier to protect the bacteria from cellular immune response and antibiotics. Consequently, cells inside the biofilm have a much higher antibiotic tolerance compared with their planktonic counterparts which makes them very difficult to eradicate [50]. In addition to *in situ* biofilm formation, pathogens with high motility such as *S. mutans* can migrate along the

dental implant interface, adhere and grow on new sites to form new colonies, and subsequently result in whole implant infection, which eventually leads to implant failure and bone loss [7,51]. Therefore, an effective way to prevent infection is to inhibit biofilm formation on the Ti implant interface, rather than attempt to remove the matured biofilms. To examine further the long-term function of the immobilized antibiotic on the pDA-coated Ti, biofilm formation within 7 days of exposure to *E. coli* and *S. mutans* was evaluated and monitored using CLSM. Figure 10 shows CLSM images of 7 day bacterial biofilms on the unmodified and modified Ti interfaces with the LIVE/DEAD BacLight bacterial viability kit. For the pristine Ti interface, extensive *E. coli* and *S. mutans* biofilm was formed and reached about 30 μm thickness with visible dead and live bacteria, consistent with SEM analysis. CLSM images show more dead *E. coli* cells than dead *S. mutans* cells on the pristine Ti interface with red colour. In sharp contrast, nearly no bacterial cells and no trace of biofilm were found on the

CS-decorated Ti interface (figure 10*b*,*d*). Furthermore, the amount of *E. coli* and *S. mutans* on the CS-decorated Ti interfaces remained at very low level (similar to the control) and did not increase with time, even if bacteria were cultured on the interfaces for almost one month as shown in the electronic supplementary material, figure S4, suggesting that the antimicrobial effectiveness of Ti-pDA-CS implant can be preserved for an extended period of time. CS is a semi-synthetic cephalosporin derivative belonging to the third-generation cephalosporins. Owing to its broad antibacterial activity and its high resistance to beta-lactamases, it is widely used for the treatment of patients with serious infections [52,53]. CS does not have serious side effects, has not caused bleeding, coagulopathy or disulfiram-like reactions [54,55] and is not nephrotoxic in humans at the therapeutic dosage [56]. Therefore, the remarkable safety record of CS is an important consideration for clinicians in the selection of an antimicrobial agent for seriously ill patients. It is currently believed that the antimicrobial mechanism of CS is ultimately dependent on the inhibition (acylation) of one or more of the bacterial penicillin-binding proteins (PBPs). The inhibition of PBPs hinders the synthesis of glycopeptide, which plays a crucial role in the formation of the cytoderm, thus resulting in bacterial cell rupture [57,58]. As a consequence, our innovative CS antibiotic immobilization using mussel-inspired pDA coating is able to confer enhanced short-term and long-term antimicrobial activity to the modified Ti substrate that is important in reducing bacterial contamination during dental implantation.

4. Conclusion

In summary, a novel antibiotic-decorated Ti substrate (or implant) with enhanced antibacterial activity has been prepared by immobilization of dopamine on the surface of Ti substrate followed by one-step self-polymerization of dopamine, and the tethering of CS, a widely used antibiotic, via catechol chemistry. XPS and static contact angle confirmed that CS was successfully grafted onto the pDA-coated Ti. After 72 h incubation, the CS-decorated Ti induced good *in vitro* antibacterial activity toward *E. coli* and *S. mutans*, Gram-negative and Gram-positive bacteria, respectively. More importantly, long-term effectiveness of the grafted CS was maintained and biofilm formation was inhibited on the interface of CS-decorated Ti with good biocompatibility and without causing significant haemolysis. Overall, compared with the pristine Ti, the CS-decorated Ti interface displayed excellent short-term and long-term antibacterial activity and could be a good candidate for dental implant and bone graft substitutes. We believe that this facile biomimetic method could offer a promising strategy for fabrication of different antibiotic-decorated Ti implants with immobilization of other antibiotics or combination of antibiotics to defend against acquired antibiotic-resistant bacteria.

References

1. Sileika TS, Kim H-D, Maniak P, Messersmith PB. 2011 Antibacterial performance of polydopamine-modified polymer surfaces containing passive and active components. *ACS Appl. Mater. Interfaces* **3**, 4602–4610. (doi:10.1021/am200978h)

2. Del Fabbro M, Testori T, Francetti L, Weinstein R. 2005 Systematic review of survival rates for implants placed in the grafted maxillary sinus. *J. Prosthet. Dent.* **94**, 266. (doi:10.1016/j.prosdent.2005.04.024)

3. Lu X et al. 2011 Nano-Ag-loaded hydroxyapatite coatings on titanium surfaces by electrochemical deposition. *J. R. Soc. Interface* **8**, 529–539. (doi:10.1098/rsif.2010.0366)

4. Mouhyi J, Dohan Ehrenfest DM, Albrektsson T. 2012 The peri-implantitis: implant surfaces, microstructure, and physicochemical aspects. *Clin. Implant Dent. Relat. Res.* **14**, 170–183. (doi:10.1111/j.1708-8208.2009.00244.x)

5. Lischer S, Körner E, Balazs DJ, Shen D, Wick P, Grieder K, Haas D, Heuberger M, Hegemann D. 2011 Antibacterial burst-release from minimal Ag-containing plasma polymer coatings. *J. R. Soc. Interface* **8**, 1019–1030. (doi:10.1098/rsif.2010.0596)

6. Broggini N, McManus L, Hermann J, Medina R, Schenk R, Buser D, Cochran D. 2006 Peri-implant inflammation defined by the implant-abutment interface. *J. Dent. Res.* **85**, 473–478. (doi:10.1177/154405910608500515)

7. Wang R, Neoh KG, Shi Z, Kang ET, Tambyah PA, Chiong E. 2012 Inhibition of *Escherichia coli* and *Proteus mirabilis* adhesion and biofilm formation on medical grade silicone surface. *Biotechnol. Bioeng.* **109**, 336–345. (doi:10.1002/bit.23342)

8. DeJong JT, Soga K, Banwart SA, Whalley WR, Ginn TR, Nelson DC, Mortensen BM, Martinez BC, Barkouki T. 2011 Soil engineering *in vivo*: harnessing natural biogeochemical systems for sustainable, multi-functional engineering solutions. *J. R. Soc. Interface* **8**, 1–15. (doi:10.1098/rsif.2010.0270)

9. Ding X, Yang C, Lim TP, Hsu LY, Engler AC, Hedrick JL, Yang Y-Y. 2012 Antibacterial and antifouling catheter coatings using surface grafted PEG-b-cationic polycarbonate diblock copolymers. *Biomaterials* **33**, 6593–6603. (doi:10.1016/j.biomaterials.2012.06.001)

10. Campoccia D, Montanaro L, Arciola CR. 2006 The significance of infection related to orthopedic devices and issues of antibiotic resistance. *Biomaterials* **27**, 2331–2339. (doi:10.1016/j.biomaterials.2005.11.044)

11. Krishnan S, Weinman CJ, Ober CK. 2008 Advances in polymers for anti-biofouling surfaces. *J. Mater. Chem.* **18**, 3405–3413. (doi:10.1039/B801491D)

12. Banerjee I, Pangule RC, Kane RS. 2011 Antifouling coatings: recent developments in the design of surfaces that prevent fouling by proteins, bacteria, and marine organisms. *Adv. Mater.* **23**, 690–718. (doi:10.1002/adma.201001215)

13. He T, Shi Z, Fang N, Neoh K, Kang E, Chan V. 2009 The effect of adhesive ligands on bacterial and fibroblast adhesions to surfaces. *Biomaterials* **30**, 317–326. (doi:10.1016/j.biomaterials.2008.09.049)

14. Wagner VE, Koberstein JT, Bryers JD. 2004 Protein and bacterial fouling characteristics of peptide and antibody decorated surfaces of PEG-poly(acrylic acid) co-polymers. *Biomaterials* **25**, 2247–2263. (doi:10.1016/j.biomaterials.2003.09.020)

15. Gottenbos B, van der Mei HC, Klatter F, Nieuwenhuis P, Busscher HJ. 2002 *In vitro* and *in vivo* antimicrobial activity of covalently coupled quaternary ammonium silane coatings on silicone rubber. *Biomaterials* **23**, 1417–1423. (doi:10.1016/S0142-9612(01)00263-0)

16. Tan XW, Lakshminarayanan R, Liu SP, Goh E, Tan D, Beuerman RW, Mehta JS. 2012 Dual functionalization of titanium with vascular endothelial growth factor and β-defensin analog for potential application in keratoprosthesis. *J. Biomed. Mater. Res. B* **100**, 2090–2100. (doi:10.1002/jbm.b.32774)

17. Kazemzadeh-Narbat M, Lai BF, Ding C, Kizhakkedathu JN, Hancock RE, Wang R. 2013 Multilayered coating on titanium for controlled release of antimicrobial peptides for the prevention of implant-associated infections. *Biomaterials* **34**, 5969–5977. (doi:10.1016/j.biomaterials.2013.04.036)

18. Ren N, Li R, Chen L, Wang G, Liu D, Wang Y, Zheng L, Tang W, Jiang H. 2012 *In situ* construction of a titanate-silver nanoparticle-titanate sandwich nanostructure on a metallic titanium surface for

bacteriostatic and biocompatible implants. *J. Mater. Chem.* **22**, 19 151–19 160. (doi:10.1039/C2JM32434B)

19. Desai DG, Liao KS, Cevallos ME, Trautner BW. 2010 Silver or nitrofurazone impregnation of urinary catheters has a minimal effect on uropathogen adherence. *J. Urology* **184**, 2565–2571. (doi:10.1016/j.juro.2010.07.036)

20. Hickok NJ, Shapiro IM. 2012 Immobilized antibiotics to prevent orthopaedic implant infections. *Adv. Drug Delivery Rev.* **64**, 1165–1176. (doi:10.1016/j.addr.2012.03.015)

21. Raad I, Reitzel R, Jiang Y, Chemaly R, Dvorak T, Hachem R. 2008 Anti-adherence activity and antimicrobial durability of anti-infective-coated catheters against multidrug-resistant bacteria. *J. Antimicrob. Chemother.* **62**, 746–750. (doi:10.1093/jac/dkn281)

22. Sun Y, Deng Y, Ye Z, Liang S, Tang Z, Wei S. 2013 Peptide decorated nano-hydroxyapatite with enhanced bioactivity and osteogenic differentiation via polydopamine coating. *Colloids Surf. B* **111**, 107–116. (doi:10.1016/j.colsurfb.2013.05.037)

23. Yang K et al. 2012 Polydopamine-mediated surface modification of scaffold materials for human neural stem cell engineering. *Biomaterials* **33**, 6952–6964. (doi:10.1016/j.biomaterials.2012.06.067)

24. Luo R, Tang L, Wang J, Zhao Y, Tu Q, Weng Y, Shen R, Huang N. 2013 Improved immobilization of biomolecules to quinone-rich polydopamine for efficient surface functionalization. *Colloids Surf. B* **106**, 66–73. (doi:10.1016/j.colsurfb.2013.01.033)

25. Shukla SK, Quraishi M. 2009 Cefotaxime sodium: a new and efficient corrosion inhibitor for mild steel in hydrochloric acid solution. *Corros. Sci.* **51**, 1007–1011. (doi:10.1016/j.corsci.2009.02.024)

26. Sharma R, Choudhary S, Kishore N. 2012 Insights into the binding of the drugs diclofenac sodium and cefotaxime sodium to serum albumin: calorimetry and spectroscopy. *Eur. J. Pharm. Sci.* **46**, 435–445. (doi:10.1016/j.ejps.2012.03.007)

27. Zhu L-P, Yu J-Z, Xu Y-Y, Xi Z-Y, Zhu B-K. 2009 Surface modification of PVDF porous membranes via poly(DOPA) coating and heparin immobilization. *Colloids Surf. B* **69**, 152–155. (doi:10.1016/j.colsurfb.2008.11.011)

28. Poh CK, Shi Z, Lim TY, Neoh KG, Wang W. 2010 The effect of VEGF functionalization of titanium on endothelial cells *in vitro*. *Biomaterials* **31**, 1578–1585. (doi:10.1016/j.biomaterials.2009.11.042)

29. Wei Q, Li B, Yi N, Su B, Yin Z, Zhang F, Li J, Zhao C. 2011 Improving the blood compatibility of material surfaces via biomolecule-immobilized mussel-inspired coatings. *J. Biomed. Mater. Res. A* **96**, 38–45. (doi:10.1002/jbm.a.32956)

30. Lee H, Dellatore SM, Miller WM, Messersmith PB. 2007 Mussel-inspired surface chemistry for multifunctional coatings. *Science* **318**, 426–430. (doi:10.1126/science.1147241)

31. Shin YM, Lee YB, Shin H. 2011 Time-dependent mussel-inspired functionalization of poly(l-lactide-co-ε-caprolactone) substrates for tunable cell behaviors. *Colloids Surf. B* **87**, 79–87. (doi:10.1016/j.colsurfb.2011.05.004)

32. Menzies DJ, Nelson A, Shen H-H, McLean KM, Forsythe JS, Gengenbach T, Fong C, Muir BW. 2012 An X-ray and neutron reflectometry study of 'PEG-like' plasma polymer films. *J. R. Soc. Interface* **9**, 1008–1019. (doi:10.1098/rsif.2011.0509)

33. Deng Y et al. 2013 Long-term self-renewal of human pluripotent stem cells on peptide-decorated poly(OEGMA-co-HEMA) brushes under fully defined conditions. *Acta Biomater.* **9**, 8840–8850. (doi:10.1016/j.actbio.2013.07.017)

34. Chen CZ, Beck-Tan NC, Dhurjati P, van Dyk TK, LaRossa RA, Cooper SL. 2000 Quaternary ammonium functionalized poly(propylene imine) dendrimers as effective antimicrobials: structure–activity studies. *Biomacromolecules* **1**, 473–480. (doi:10.1021/bm0055495)

35. Saidin S, Chevallier P, Abdul Kadir MR, Hermawan H, Mantovani D. 2013 Polydopamine as an intermediate layer for silver and hydroxyapatite immobilisation on metallic biomaterials surface. *Mater. Sci. Eng. C* **33**, 4715–4724. (doi:10.1016/j.msec.2013.07.026)

36. Hunt PR, Marquis BJ, Tyner KM, Conklin S, Olejnik N, Nelson BC, Sprando RL. 2013 Nanosilver suppresses growth and induces oxidative damage to DNA in *Caenorhabditis elegans*. *J. Appl. Toxicol.* **33**, 1131–1142. (doi:10.1002/jat.2872)

37. Albers CE, Hofstetter W, Siebenrock KA, Landmann R, Klenke FM. 2013 *In vitro* cytotoxicity of silver nanoparticles on osteoblasts and osteoclasts at antibacterial concentrations. *Nanotoxicology* **7**, 30–36. (doi:10.3109/17435390.2011.626538)

38. Lynge ME, van der Westen R, Postma A, Städler B. 2011 Polydopamine: a nature-inspired polymer coating for biomedical science. *Nanoscale* **3**, 4916–4928. (doi:10.1039/C1NR10969C)

39. Jiang J, Zhu L, Zhu L, Zhu B, Xu Y. 2011 Surface characteristics of a self-polymerized dopamine coating deposited on hydrophobic polymer films. *Langmuir* **27**, 14 180–14 187. (doi:10.1021/la202877k)

40. Aslan S, Loebick CZ, Kang S, Elimelech M, Pfefferle LD, Van Tassel PR. 2010 Antimicrobial biomaterials based on carbon nanotubes dispersed in poly(lactic-co-glycolic acid). *Nanoscale* **2**, 1789–1794. (doi:10.1039/C0NR00329H)

41. Rodríguez-Valverde MA, Ruiz-Cabello FJM, Cabrerizo-Vílchez MA. 2011 A new method for evaluating the most-stable contact angle using mechanical vibration. *Soft Matter* **7**, 53–56. (doi:10.1039/C0SM00939C)

42. Ku SH, Ryu J, Hong SK, Lee H, Park CB. 2010 General functionalization route for cell adhesion on non-wetting surfaces. *Biomaterials* **31**, 2535–2541. (doi:10.1016/j.biomaterials.2009.12.020)

43. Sun K, Xie Y, Ye D, Zhao Y, Cui Y, Long F, Zhang W, Jiang X. 2012 Mussel-inspired anchoring for patterning cells using polydopamine. *Langmuir* **28**, 2131–2136. (doi:10.1021/la2041967)

44. Rim NG, Kim SJ, Shin YM, Jun I, Lim DW, Park JH, Shin H. 2012 Mussel-inspired surface modification of poly(l-lactide) electrospun fibers for modulation of osteogenic differentiation of human mesenchymal stem cells. *Colloids Surf. B* **91**, 189–197. (doi:10.1016/j.colsurfb.2011.10.057)

45. Nie F, Zheng Y, Wei S, Wang D, Yu Z, Salimgareeva G, Polyakov A, Valiev R. 2012 *In vitro* and *in vivo* studies on nanocrystalline Ti fabricated by equal channel angular pressing with microcrystalline CP Ti as control. *J. Biomed. Mater. Res. A* **101**, 1694–1707. (doi:10.1002/jbm.a.34472)

46. Kaplan J. 2010 Biofilm dispersal: mechanisms, clinical implications, and potential therapeutic uses. *J. Dent. Res.* **89**, 205–218. (doi:10.1177/0022034509359403)

47. Stickler D, Lear J, Morris N, Macleod S, Downer A, Cadd D, Feast W. 2006 Observations on the adherence of *Proteus mirabilis* onto polymer surfaces. *J. Appl. Microbiol.* **100**, 1028–1033. (doi:10.1111/j.1365-2672.2006.02840.x)

48. Brauer DS, Karpukhina N, Kedia G, Bhat A, Law RV, Radecka I, Hill RG. 2013 Bactericidal strontium-releasing injectable bone cements based on bioactive glasses. *J. R. Soc. Interface* **10**, 20120647. (doi:10.1098/rsif.2012.0647)

49. Watnick P, Kolter R. 2000 Biofilm, city of microbes. *J. Bacteriol.* **182**, 2675–2679. (doi:10.1128/JB.182.10.2675-2679.2000)

50. Cazander G, van de Veerdonk MC, Vandenbroucke-Grauls CM, Jukema GN. 2010 Maggot excretions inhibit biofilm formation on biomaterials. *Clin. Orthop. Relat. Res.* **468**, 2789–2796. (doi:10.1007/s11999-010-1309-5)

51. Jacobsen S, Stickler D, Mobley H, Shirtliff M. 2008 Complicated catheter-associated urinary tract infections due to *Escherichia coli* and *Proteus mirabilis*. *Clin. Microbiol. Rev.* **21**, 26–59. (doi:10.1128/CMR.00019-07)

52. Wetterich U, Mutschler E. 1995 Quality of cefotaxime sodium preparations. *Arzneimittel-Forsch.* **45**, 74–80.

53. Vasiliu S, Bunia I, Racovita S, Neagu V. 2011 Adsorption of cefotaxime sodium salt on polymer coated ion exchange resin microparticles: kinetics, equilibrium and thermodynamic studies. *Carbohyd. Polym.* **85**, 376–387. (doi:10.1016/j.carbpol.2011.02.039)

54. Parker RH, Park S-Y. 1984 Safety of cefotaxime and other new β-lactam antibiotics. *J. Antimicrob. Chem.* **14**, 331–335. (doi:10.1093/jac/14.suppl_B.331)

55. Fekety FR. 1990 Safety of parenteral third-generation cephalosporins. *Am. J. Med.* **88**, S38–S44. (doi:10.1016/0002-9343(90)90326-9)

56. Morris DD, Rurkowski J, Lloyd KK. 1987 Therapy in two cases of neonatal foal septicaemia and meningitis with cefotaxime sodium. *Equine Vet. J.* **19**, 151–154. (doi:10.1111/j.2042-3306.1987.tb02614.x)

57. My NH, Hirao H, Van DU, Morokuma K. 2011 Computational studies of bacterial resistance to β-lactam antibiotics: mechanism of covalent inhibition of the penicillin-binding protein 2a (PBP2a). *J. Chem. Inf. Model.* **51**, 3226–3234. (doi:10.1021/ci2004175)

58. Dzhekieva L, Kumar I, Pratt R. 2012 Inhibition of bacterial DD-peptidases (penicillin-binding proteins) in membranes and *in vivo* by peptidoglycan-mimetic boronic acids. *Biochemistry* **51**, 2804–2811. (doi:10.1021/bi300148v)